physica status solidi (a)

RESEARCH ARTICLE OPEN ACCESS

Advancing Retina Implant Concepts: Assessing the Design and Validation of Origami-Type Epiretinal Implants by Computational Modeling

Eashika Ghosh[1] | Yuli Wu[2] | Hocine Bahri[1] | Vivek Pachauri[1] | Ziyu Gao[1] | Johannes Stegmaier[2] | Sven Ingebrandt[1]

[1]Institute of Materials in Electrical Engineering I (IWE1), RWTH Aachen University, Aachen, Germany | [2]Institute of Imaging & Computer Vision (LFB), RWTH Aachen University, Aachen, Germany

Correspondence: Sven Ingebrandt (ingebrandt@iwe1.rwth-aachen.de)

Received: 5 January 2026 | **Revised:** 4 July 2026 | **Accepted:** 5 July 2026

Keywords: epiretinal implants | field of view | origami-type | spatial resolution | visual recognition

ABSTRACT

We describe the modeling of a novel, foldable epiretinal implant to enhance visual perception, addressing current implant limitations of a low number of active electrodes, low spatial resolution, limited visual field, poor visual recognition, and severe surgical complications. Generally, the classical development of a new implant with experimental validation followed by animal and human trials is tedious. We utilize a simulation framework that uses axon map models generated from human trials to predict the neural activation upon epiretinal stimulation with a new implant. We propose a novel, origami-type design for enhanced performance and compare it to two existing designs. The simulations assess spatial resolution and area coverage of the visual percepts. A hexagonal, foldable, origami-type design could significantly improve spatial resolution and field of view. An accuracy of 94.81% in letter recognition and a 38° field of view would be achievable with an optimal structure of this implant concept. The design's flexibility would also facilitate minimally invasive surgery with a small scleral incision through which the folded implant could be inserted and left to autonomously unfold within the eye. Our findings underscore the importance of advanced computational tools in optimizing retinal prostheses, paving the way for future vision restoration technologies.

1 | Introduction

Visual perception is our most important sense and a remarkable neurobiological process that allows us to interpret the world through our eyes. However, for numerous individuals who are affected by diseases like Retinitis Pigmentosa (RP) or age-related macular degeneration, the ability to perceive visual input can be significantly reduced.

RP causes a gradual breakdown of photoreceptor cells, often starting with a drastically reduced field of view (i.e., tunnel vision), progressing toward significant vision loss with complete blindness in the end-stage. Although there have been advancements in gene therapy and neuroprotective treatments, there is still no cure for late-stage RP. Interestingly, research shows that bipolar neurons and 30% of the ganglion cells in the retina remain active even after the photoreceptor cells are entirely damaged [1, 2]. This opens up possibilities to restore vision by electrical stimulation of the surviving cells, which is the basis to develop of electrical retinal prostheses.

Among other notable implant concepts like subretinal and suprachoroidal implants, this study focuses on the epiretinal implant approach [3]. This concept aims to directly stimulate ganglion cells by bypassing all other cells, reducing the likelihood of serious surgical complications [4]. One of the most significant advancements in this field is the Argus II, the first commercially available epiretinal implant [5]. It has been shown that artificial vision is possible with this device, offering hope for persons with severe visual impairments. However, it also became evident that the Argus II has limitations, including a too narrow field of view and too low spatial resolution, which hinder users' abilities to perform everyday tasks like reading or recognizing faces [6]. Due to the specific morphology of the retina with axons of neighboring ganglion cells running along specific tracks, the patients reported phosphenes with particular elliptic shapes. This is a pivotal challenge of all epiretinal concepts, since shape, size, and angle of these phosphenes depend on the placement and coupling of each electrode and on the individual morphology of each patient's retina. For better visual perception, next-generation epiretinal implants must incorporate a higher number of electrodes while covering a larger area to expand the field of view. The optimized placement should be simulated and tested, where advanced simulation methods might aid better comprehension of the underlying mechanisms. A large area implant should still allow for an easy implantation procedure in order to keep the surgical trauma to the eye at a minimum.

A significant challenge in retinal prostheses is the number of electrodes, which directly affects visual quality [7]. The Argus II only has 60 electrodes, resulting in a low-resolution and pixelated visual perception [6]. Increasing the number of electrodes would dramatically improve visual clarity, aiding shape recognition and object detection [8]. Newer designs, such as the very large electrode arrays for retinal stimulation (VLARS), aimed to tackle this limitation by utilizing 250 stimulating pixels [9]. However, simply increasing the number of electrodes is not enough; keeping the surgical procedures as easy as possible is an additional constraint in the implant design [10].

We propose a novel, foldable, origami-type dense electrode array for retinal stimulation (DEARS) to meet these challenges (Figure 1). This conceptual approach would allow for higher electrode densities, while ensuring minimal surgical invasion. Computational models suggest that denser arrays would produce sharper phosphenes, enabling a better performance in tasks like letter identification and Braille code reading, which is the dot-like letter concept to enable blind persons to read text with their fingers [11]. The combined improvement of field of view, enhanced resolution, and ease of surgery would represent a next-generation of epiretinal implants. The Argus II is the first FDA-approved retinal implant. It utilizes a 6×10 rectangular electrode grid to reach a 20° field of view, but with limited visual resolution. In earlier works of our institute, the VLARS concept was developed, but it never made it into the eyes of human patients. It offers 250 electrodes integrated in a round shape using a flexible 12 mm array with a field of view of 18.8°, theoretically improving field of view and shape recognition, simultaneously [9].

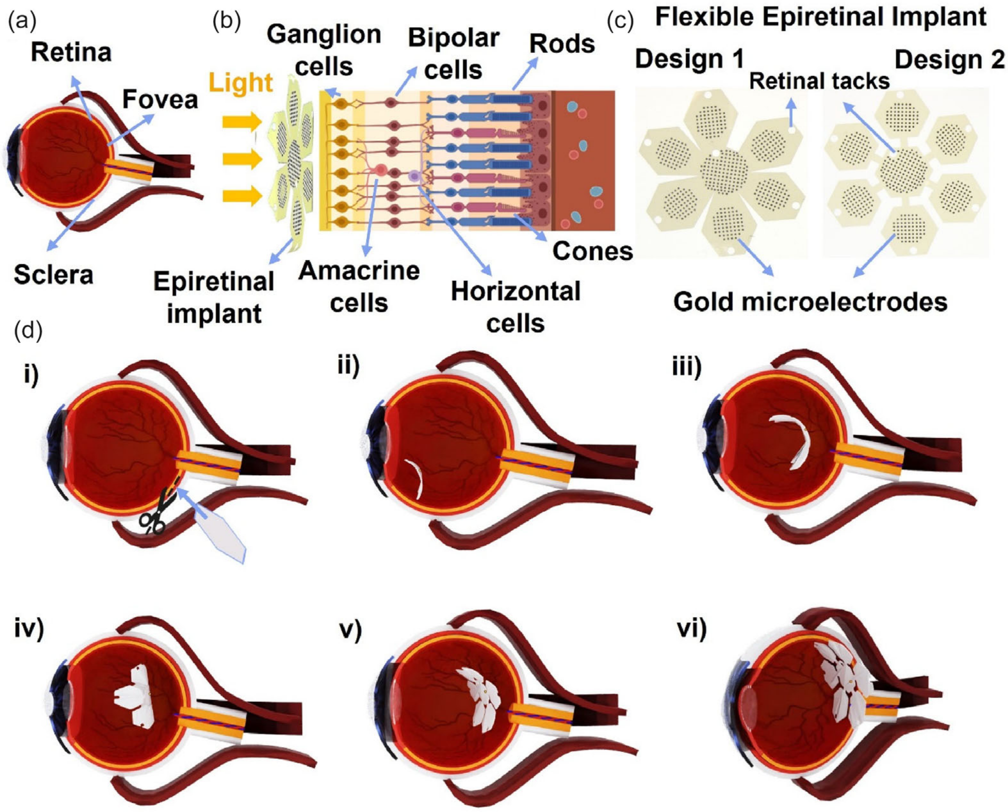

FIGURE 1 | Schematic illustration of the DEARS design as a foldable epiretinal implant: (a) An image of the eye is shown, indicating the locations of the retina, fovea, and sclera. (b) The figure illustrates the epiretinal design that is placed onto the surface of the retina. (c) The image presents two origami-inspired designs suitable for the epiretinal approach. (d) The folding and unfolding of the implant structure are explained in (i–vi). i) A small incision of approximately 2.5–3 mm should be made within the vitreous area, allowing the folded implant to be gradually slid into the eye. ii–v) The sequence depicts the detailed progression of the implant as it unfolds inside the eye. vi) Ultimately, the structure unfolds completely and conforms to the curved shape of the retina, resting on its surface ready for later fixation.

Generally, the implantation of large epiretinal devices is a significant challenge. Traditional implants are rigid, requiring large incisions, increasing the risk of tissue damage and post-surgical complications. Given the delicate and curved structure of the human eye, placing and fixating traditional implants is technically challenging. Conventional devices necessitate larger surgical incisions, leading to higher risks of inflammation and misalignment. Plus, the flat electrode arrays create uneven contacts to the curved retina with large electrode-tissue distances and hence reduce the effectiveness of stimulation [12].

Origami-inspired, foldable epiretinal implants would be a leap forward in retinal prosthesis technology. The innovative design facilitates easy folding, enabling insertion through a minimal incision. When the implant structure is unfolded from its smaller form, it should better adapt to the curvature of the retina, thus ensuring optimal alignment and contact with the ganglion cell layer of the retina. This concept would significantly reduce surgical complexity and trauma, while enhancing the accuracy of electrode placement and promoting long-term stability. Overall, an origami-type implant concept promises improved visual restoration. However, the pipeline of implant development, characterization, validation, and approval of clinical trials is very long and tedious.

In this study, we explored the technological prospect of such a novel, foldable implant from a theoretical viewpoint. Therefore, we examined two novel, foldable electrode array designs and compared them to two already existing designs. We evaluated the distinguishability of the predicted visual perceptions using the simulation library Pulse2Percept [13]. This framework uses a physiologically validated computational model, the axon map model, including optimized parameters from earlier experiments with patients wearing Argus II implants [14]. With the three epiretinal implant designs, namely Argus II, VLARS, and DEARS, we conducted simulations to acquire the predicted perceptions with a grayscale dataset containing handwritten letters. We compared three different modes to arrange the stimulations on the electrode arrays: letter-only, Braille code only, and a combination of both.

2 | Materials and Methods

2.1 | Novel Design of the Implant

We designed two foldable test arrays with a large surface area (9 mm in width), which could potentially accommodate a large number of electrodes. These test arrays are not functional yet, but are utilized for implantation tests. Two hexagonal-shaped substrate structures were designed to investigate origami-type folding properties (Figure 1c). The foldable wings of the hexagonal electrode arrays would be located in the perifoveal region of the retina, while the central part would address the fovea. One wing measures 2.5 mm in diameter containing 60 electrodes. With 6 wings and 120 electrodes in the fovea region, the foldable implant structure accommodates 480 electrodes in total.

2.2 | Axon Map Model

We utilized the physiologically validated simulation tool Pulse2Percept [13], including the axon map model [14], for our theoretical considerations. Two parameters, ρ and λ, play an important role in the shape of the elliptical phosphenes elicited by electronic stimulation, as illustrated in Figure 2a. The parameter ρ depicts the area around the stimulated electrode, and λ depicts the length of the elongated tail along the axon. This specific shape of stimulated phosphenes is a result of earlier experiments with patients wearing Argus II implants. For our simulations, we used two sets of ρ and λ to represent an idealized case ($\rho = 150\,\mu\text{m}$, $\lambda = 500\,\mu\text{m}$) and a realistic case ($\rho = 410\,\mu\text{m}$, $\lambda = 1190\,\mu\text{m}$), which are based on data of a real patient implanted with Argus II [14].

2.3 | Convolutional Neural Network

We employed a simple visual geometry group (VGG)-style [15] neural network to recognize the predicted percepts and to simulate the expected visual perception of patients. As shown in Figure 2b, the neural network consists of three convolutional layers, two max-pooling layers, and two dense layers with dropout. The depth of each feature map is denoted in Figure 2b. At the end of the neural network, we used the cross-entropy loss with a softmax activation. With this classification task, we evaluated the distinguishability with the accuracy metric.

2.4 | Dataset

To evaluate potential letter recognition, we utilized the dataset "Extended Modified National Institute of Standards and Technology database" EMNIST [16], which contains grayscale uppercase or lowercase letters of 28×28 pixels. We randomly selected 100 images for each of the 26 case-independent letters to build a dataset of 2,600 images for the simulations. Fractions of 80% and 20% were randomly chosen as training and test sets, respectively. Both sets were balanced in terms of each letter. The classification accuracy on the test set is shown in Table 1 and Figure 3. Two examples of the original images from EMNIST are displayed in Figure 3.

3 | Results and Discussion

Earlier studies have shown that the fovea, which is specialized for high-acuity vision serving as the focal point for our conscious visual experience, occupies only a small area of the retina (shown in Figure 1a) of less than the size of a thumbnail at arm's length [17].

In our foldable implant concept, the area of the fovea is densely addressed with 120 electrodes of 100 μm in diameter. The electrodes are spaced in round-shaped arrays on each wing and central area, particularly leaving a large space between wings and the central area. Leaving this space free is pivotal to allow for folding and unfolding without harming the electrodes. Contact lines

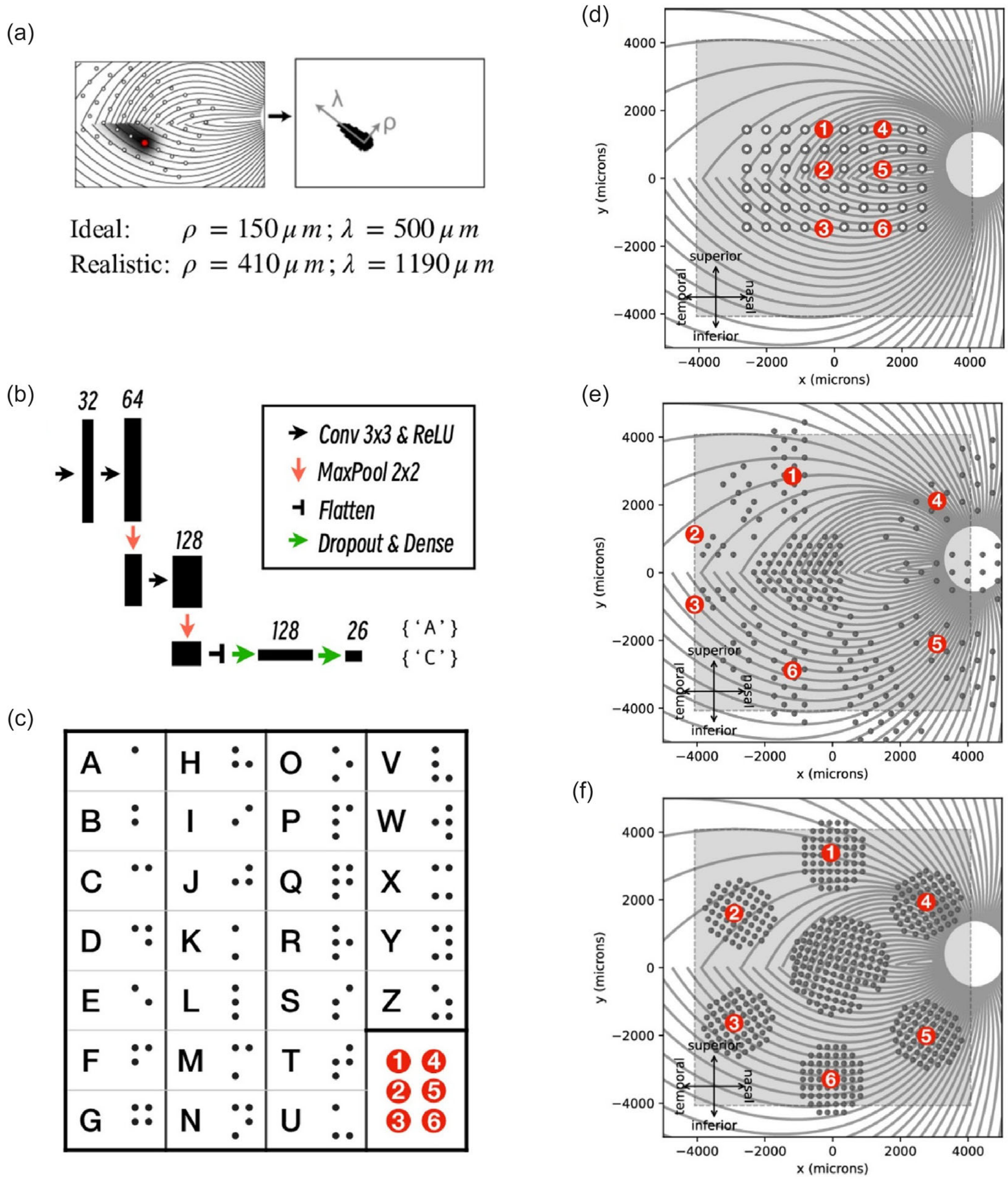

FIGURE 2 | Axon map comparison of the three retinal implant designs Argus II, VLARS and DEARS: (a) An illustration of the axon map model with two sets of the parameters of an idealized case and a realistic case (adapted from [14]). (b) The architecture of the neural network for the classification task. (c) The standard 6-bit Braille codes for 26 letters used in this work. (d–f) The layouts of the implants, Argus II (d), VLARS (e), and DEARS (f) on an axon map model of the retina. Lines represent axons projecting into the central visual nerve on the right side. The red circles represent the corresponding Braille code nodes, as listed in (c). The figures were plotted using the Pulse2Percept tool [13].

should be foldable without degradation, which was analyzed by another work within the epiretinal implant consortium [18].

Six wings of hexagonal shape can fold and unfold from this central area. As described above, the DEARS implant carries 480 electrodes, significantly exceeding the electrode counts of VLARS and Argus II, thereby providing an improved spatial resolution. During surgery, the origami-type implant could be folded into a small size of just 2.5 mm. Thereby, the implant could be inserted into the eye via a tiny incision of about 2.5–3 mm in the sclera. Upon entering the vitreous cavity, the structure should autonomously unfold due to its unique design, positioning itself in a manner that aligns comfortably with the retina, ready for fixation at the tissue surface.

The whole folding and unfolding process is systematically shown in the figure sequence i–vi of Figure 1d. This functionality would be ideal for a large-area, high–density interface with the retinal tissue. The flexible nature of the implant, along with the use of biocompatible materials such as Parylene-C, would allow it to conform closely to the curved shape of the retina. Additionally, with a total diameter of 9 mm, the central implant area effectively covers the foveal part of the retina, while the unfolded wings offer an increased visual angle of about 38°. This concept could enhance the development of retinal prosthetics addressing both the spatial resolution and the field of view. Different from other approaches to optimize the retinal prosthetic stimulations [19–21], we directly evaluated the distinguishability (or recognizability) of the predicted percepts based

TABLE 1 | Classification accuracy of the simulated percepts with different experimental parameters, including three retinal implants, two sets of axon map model parameters, and three modes of stimulation. The indices are in accordance with the visualizations in Figure 3.

	Simulation	Parameters			Accuracy, %		
Implants	rho, µm	lambda, µm	Letter	Braille code	Epoch 1	Epoch 10	Index
Argus II	150	500	Yes	No	20.19	58.08	I
	150	500	No	Yes	100.00	100.00	II
	410	1190	Yes	No	6.73	38.46	III
	410	1190	No	Yes	80.77	100.00	IV
VLARS	150	500	Yes	No	29.62	60.00	V
	150	500	No	Yes	88.46	100.00	VI
	150	500	Yes	Yes	74.23	100.00	VII
	410	1190	Yes	No	18.65	50.96	VIII
	410	1190	No	Yes	73.08	100.00	IX
	410	1190	Yes	Yes	69.62	100.00	X
DEARS	150	500	Yes	No	22.31	53.85	XI
	150	500	No	Yes	92.31	100.00	XII
	150	500	Yes	Yes	94.81	100.00	XIII
	410	1190	Yes	No	21.15	54.04	XIV
	410	1190	No	Yes	88.46	100.00	XV
	410	1190	Yes	Yes	92.31	100.00	XVI

on trivial downsampling or Braille encoding. A pair of one percept and one letter class was trained with a supervised classification task [22]. The advantages of our newly designed epiretinal implant can be demonstrated with these in silico experiments. The simulations are indexed with roman numbers from I to XVI, as listed in Table 1, and are shown in Figure 3. All three epiretinal implant concepts are positioned on top of the retina as visualized in Figure 1. The general concept of all epiretinal implants is the direct stimulation of the large ganglion cells bypassing the other neuronal layers. Targeting the retina epiretinally has shown benefits in terms of surgical feasibility and relatively low risks compared to stimulation of the visual cortex or the optic nerve [9, 10].

3.1 | Argus II

The Argus II implant with its 60 electrodes and visual acuity of 20/1260 was the first approved device for clinical trials in the United States (FDA phase 4, post-market surveillance) and in Europe (phase IV, European CE marking) [23, 24]. The first model, Argus I, consisted of 16 electrodes and was implanted in six subjects. The improved version, Argus II, consists of a 60-electrode array and has so far been implanted in 30 subjects for up to 38.3 months, with 94.4% of electrodes retaining their function throughout the study. 29 patients continued home use of the device. Out of the clinical analysis of this implant concept, the simulation tool Pulse2Percept, including the axon map model, was developed [13].

3.2 | Vision Restoration

Testing of Argus II included locating objects, identifying motion direction, reading letters, orientation, and mobility tasks. A convincing number of 21 of 28 patients performed better with the implant in its on-state versus the off-state, with an estimated field of view of 22. Moreover, on the grating visual acuity (GVA) test, Argus II subjects scored 1.6 and 2.9 LogMAR (logarithm of the minimum angle of resolution) when the system is in the on-state [5, 25]. Furthermore, tracing paths on touchscreens with auditory feedback had higher accuracy, but longer decision times with the implant in its on-state. This was explained by earlier learning and eventual reactivation of the visual pathway [6].

3.3 | VLARS

This back-illuminated, flexible, CMOS-based photodiode array with customized, thinned silicon chips embedded into flexible polyimide was developed in IWE1 in the framework of an earlier project [9]. The VLARS array measures 12 mm in diameter and covers an area of approximately 110 mm^2, resulting in a visual angle of 37.6° and a field of view of 18.8°, respectively. Two designs were realized containing 250 individual electrodes, each having a diameter of 100 µm except the larger return electrode at the base of the array's connecting lead. The electrodes' density increased toward the array's center with an average pitch of 300 µm [9, 10]. This implant concept was developed but was not mature enough to be utilized in clinical trials. However, with the simulation framework as described in this study, its performance compared to the other concepts can be anticipated.

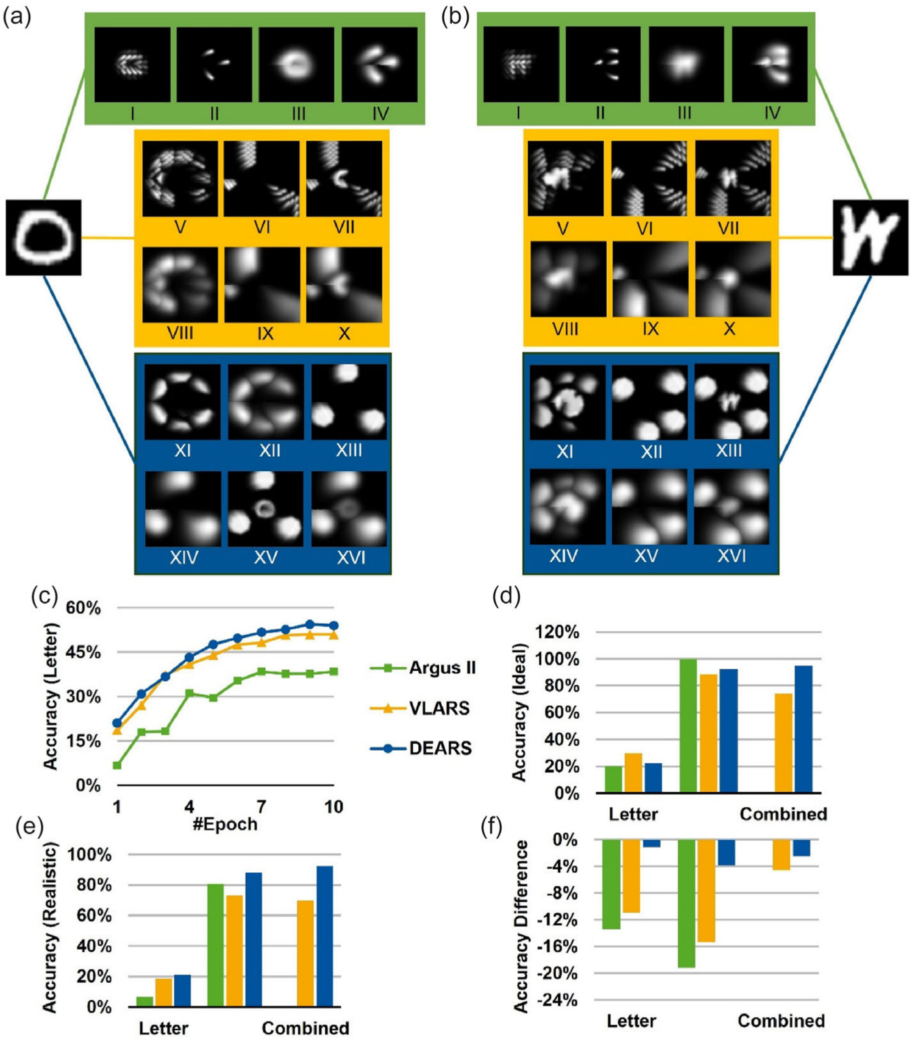

FIGURE 3 | Recognition accuracy modeling and comparison of the three implant concepts: (a,b) The visualization of two representative examples of letters O and W according to Argus II (green), VLARS (yellow), and DEARS (blue). (c) A comparison of the classification accuracy on the realistic letters using three retinal implants in terms of the number of epochs. (d) The classification accuracy with idealized computational parameters using the three retinal implants after the first epoch. (e) The classification accuracy with realistic computational parameters using three retinal implants after the first epoch. (f) The difference in classification accuracy from idealized to realistic computational parameters using Argus II, VLARS, and DEARS after the first epoch.

3.4 | DEARS

The foldable, origami-type, flexible implant designed and validated within this study has a diameter of 9 mm and consists of 480 microelectrodes, 60 electrodes in each of the peripheral leaves and 120 electrodes in the center targeting the fovea. The diameter of the electrodes was kept the same as in the VLARS implant, resulting in a visual angle of 38°. Due to the folding concept, the electrodes of the six blades and the central area are separated, leading to a sparse array. Within the simulations presented here, we wanted to address whether, despite this separation, an acceptable visual perception can be expected.

3.5 | Simulation Experiments

To test the expected capabilities of the different designs, we performed different stimulation experiments, where input images were converted to implant stimuli and then translated to visual percepts using the Pulse2Percept library. We generated the predicted percepts in three scenarios: letter- only, Braille code only, and combined. With the stimulation as the input of the axon map model using Pulse2Percept, the predicted percept was generated and resized to the same size as the original letter image (28×28 pixels). All networks were trained in a supervised manner for 10 epochs, and accuracy scores were reported based on the test sets after each epoch.

3.6 | Letter Recognition Simulation

The letter image was first downsampled to match the resolution of the electrode arrays without changing its proportions. Each electrode was then stimulated with an amplitude corresponding to the respective pixel intensity.

3.7 | Braille Code Reading Simulation

Encoding an epiretinal electrode array with Braille codes has been proven to improve the reading performance, a finding validated since the early days of Argus II [11]. Following this concept, we selected six electrodes as the Braille code nodes, as illustrated in Figure 2d–f. Thanks to the higher resolution of the VLARS and DEARS implants, we were able to select larger areas to represent the Braille codes, as illustrated in Figure 2e,f. The generation of the predicted percepts was then the same as in the letter-only simulation.

3.8 | Combined Simulation With Letters and Braille Codes

Due to the limited resolution of Argus II, it was not possible to display both letters and Braille codes. Nevertheless, we compared all three array concepts and left out the combined case for Argus II. We combined letters and Braille codes in one stimulation, while letters were projected to the foveal region and Braille codes were displayed in the peripheral region.

3.9 | Recognition Accuracy

The recognition accuracy of the supervised classification task is listed in Table 1 for 16 simulation experiments indexed from I to XVI. The corresponding visualization is showcased in Figure 3a,b with two representative images "O" and "W". We compared the classification accuracy with respect to the number of epochs in the letter-only simulation experiments with the realistic ρ and λ values. The DEARS implant performed slightly better than the VLARS implant and, thanks to its higher number of electrodes, considerably better than the Argus II implant.

After the first epoch, the classification accuracy values for idealized and realistic axon map model parameters are shown in Figure 3c,d, respectively. With the help of Braille codes, the accuracy can be significantly improved compared to letter-only cases. The DEARS implant outperforms both the Argus II and the VLARS implant consistently when the ρ and λ values of the realistic case are considered (Figure 3e).

3.10 | Robustness

In Figure 3f, the differences in classification accuracy from idealized to realistic computational parameters are compared with all three retinal implants, which can be interpreted as the robustness of each implant toward increased ρ and λ values, i.e., larger phosphenes than in the ideal case. The less the drop is, the more robust the retinal implant performs. Compared to Argus II and VLARS, the DEARS implant concept also shows the least accuracy declines in the three simulation experiments of letter-only, Braille code only, and combined.

4 | Conclusion

We presented and discussed an innovative epiretinal implant concept inspired by the origami-type folding technique aimed to address the current challenges of existing retinal prostheses. We assessed the anticipated performance of this implant in a simulation framework using a tool for the generation of phosphenes on an axon map combined with a neuronal network image recognition to assess possible visual recognition. Our novel implant design promises enhanced spatial resolution, an expanded field of view, and improved surgical feasibility compared to earlier designs. By integrating computational modeling, explicitly the Pulse2Percept and axon map model frameworks, we assessed the performance of our proposed implant against two other designs, the Argus II and the VLARS implants. Our findings indicate that the unique hexagonal configuration, featuring a larger number of electrodes, should yield improved visual representations and a better field of view. Thereby, the increased number of electrodes and the larger space available in the DEARS concept for the individual electrode placement can be accounted for the better performance in letter recognition compared to the other implant concepts.

Our simulation experiments provided compelling evidence of the effectiveness of the novel implant concept. In terms of letter recognition accuracy, the Argus II implant achieved 58.08%, while the VLARS implant showed an improvement to 74.23%. Notably, the DEARS implant outperformed both, reaching an impressive accuracy of 94.81% after just 10 training epochs. However, we like to note that these values reflect the distinguishability of simulated percepts using a trained classifier, rather than a direct measure of human visual performance. The introduction of Braille encoding generally increased the recognition outcomes, where the DEARS implant attained 100% accuracy across multiple scenarios. Moreover, the visual angle of the DEARS implant of approximately 38° significantly surpassed that of the Argus II (~20°) and the VLARS implants (~37.6°), offering users a broader visual field for enhanced navigation and perception. Additionally, the DEARS implant demonstrated remarkable robustness against variations in neural activation, which corresponds to larger activation cones of phosphenes, exhibiting the smallest decline in accuracy, thereby underscoring its stability and adaptability across different conditions. This study highlights the crucial interplay of computational modeling to realize advanced microelectrode design concepts. Our future efforts will focus on the fabrication of the DEARS implant and its characterization. Here, we expect that the folding might add additional stress to the metal contact lines and might impact the overall long-term stability of the materials. For these experiments, we plan in vitro and in vivo validations. We hope that the next-generation retinal implants can be more effective and practical for real-world applications and help patients with improved artificial vision.

Author Contributions

Eashika Ghosh and **Yuli Wu** contributed equally in conceptualization and experimental analysis. **Eashika Ghosh** contributed particularly to the electrode design while **Yuli Wu** contributed to the vision simulation. Both contributed to the data analysis. **Hocine Bahri** supported on the layout sketching. **Vivek Pachauri** contributed to the funding acquisition and to supervision. **Ziyu Gao** contributed to the project design and experimental supervision. **Johannes Stegmaier and Sven Ingebrandt** contributed to the funding acquisition, project lead and supervision of the doctoral thesis works of **Yuli Wu** and **Eashika Ghosh**. All authors contributed to the data analysis, discussion and manuscript writing.

Acknowledgments

The authors sincerely thank the Deutsche Forschungsgemeinschaft (DFG) for funding this research through the Innovative Retinal Interfaces for Optimized Artificial Vision - InnoRetVision project (424556709) [26].

Open Access funding enabled and organized by Projekt DEAL.

Funding

This work was supported by the Deutsche Forschungsgemeinschaft (424556709).

Data Availability Statement

The data that support the findings of this study are available from the corresponding author upon reasonable request.

References

1. C. Koch, W. Mokwa, M. Goertz, and P. Walter, "First Results of a Study on a Completely Implanted Retinal Prosthesis in Blind Humans," in *IEEE Sensors 2008* (2008).

2. J. D. Weiland and M. S. Humayun, "Retinal Prosthesis," *IEEE Transactions on Biomedical Engineering* 61 (2014): 1412–1424, https://doi.org/10.1109/tbme.2014.2314733.

3. E. Bloch, Y. Luo, and L. da Cruz, "Advances in Retinal Prosthesis Systems," *Therapeutic Advances in Ophthalmology* 11 (2019): 1–16, https://doi.org/10.1177/2515841418817501.

4. P. Pavlova, J. Boneva, and I. Shandurkov, "Epiretinal vs. Subretinal Implant in Surgical Treatment of Retinitis Pigmentosa – A Review," *Bulgarian Review of Ophthalmology* 63 (2019): 13–18, https://doi.org/10.14748/bro.v63i1.5814.

5. L. da Cruz, B. F. Coley, J. Dorn, et al., "The Argus II Epiretinal Prosthesis System Allows Letter and Word Reading and Long-Term Function in Patients with Profound Vision Loss," *British Journal of Ophthalmology* 97 (2013): 632–636, https://doi.org/10.1136/bjophthalmol-2012-301525.

6. H. C. Stronks and G. Dagnelie, "The Functional Performance of the Argus II Retinal Prosthesis," *Expert Review of Medical Devices* 11 (2013): 23–30, https://doi.org/10.1586/17434440.2014.862494.

7. A. C. Weitz, D. Nanduri, M. R. Behrend, et al., "Improving the Spatial Resolution of Epiretinal Implants by Increasing Stimulus Pulse Duration," *Science Translational Medicine* 7 (2015): 1–11, https://doi.org/10.1126/scitranslmed.aac4877.

8. K. Y. Wu, M. Mina, J. Y. Sahyoun, A. Kalevar, and S. D. Tran, "Retinal Prostheses: Engineering and Clinical Perspectives for Vision Restoration," *Sensors (Basel)* 23 (2023): 5782, https://doi.org/10.3390/s23135782.

9. F. Waschkowski, S. Hesse, A. C. Rieck, et al., "Development of Very Large Electrode Arrays for Epiretinal Stimulation (VLARS)," *Biomedical Engineering Online* 13 (2014): 1–15, https://doi.org/10.1186/1475-925x-13-11.

10. T. K. Lohmann, F. Haiss, K. Schaffrath, et al., "The Very Large Electrode Array for Retinal Stimulation (VLARS) - A Concept Study," *Journal of Neural Engineering* 16 (2019): 1–15, https://doi.org/10.1088/1741-2552/ab4113.

11. T. Z. Lauritzen, J. Harris, S. Mohand-Said, et al., "Reading Visual Braille with a Retinal Prosthesis," *Frontiers in Neuroscience* 6 (2012): 1–7, https://doi.org/10.3389/fnins.2012.00168.

12. K. Schaffrath, T. Lohmann, J. Seifert, et al., "New Epiretinal Implant with Integrated Sensor Chips for Optical Capturing Shows a Good Biocompatibility Profile In Vitro and In Vivo," *Biomedical Engineering Online* 20 (2021): 1–20, https://doi.org/10.1186/s12938-021-00938-9.

13. M. Beyeler, G. M. Boynton, I. Fine, and A. Rokem, "pulse2percept: A Python-based Simulation Framework for Bionic Vision," in *15th Python in Science Conference Austin* (2017), https://www.biorxiv.org/content/biorxiv/early/2017/07/10/148015.full.pdf.

14. M. Beyeler, D. Nanduri, J. D. Weiland, A. Rokem, G. M. Boynton, and I. Fine, "A Model of Ganglion Axon Pathways Accounts for Percepts Elicited by Retinal Implants," *Scientific Reports* 9 (2019): 1–16, https://doi.org/10.1038/s41598-019-45416-4.

15. K. S. A. Zisserman, "Very Deep Convolutional Networks for Large-Scale Image Recognition," in *International Conference on Learning Representations* (2015), http://arxiv.org/pdf/1409.1556.

16. G. Cohen, S. Afshar, J. Tapson, and A. van Schaik, "EMNIST: Extending MNIST to handwritten letters," in *International Joint Conference on Neural Networks (IJCNN)*, (2017).

17. J. E. McGregor, "Restoring Vision at the Fovea," *Current Opinion in Behavioral Sciences* 30 (2019): 210–216, https://doi.org/10.1016/j.cobeha.2019.10.003.

18. M. Jung, J. Abu Shihada, S. Decke, et al., "Flexible 3D Kirigami Probes for In Vitro and In Vivo Neural Applications," *Advanced Materials* 37 (2025): 1–21, https://doi.org/10.1002/adma.202418524.

19. J. Granley, L. Relic, and M. Beyeler, "Hybrid Neural Autoencoders for Stimulus Encoding in Visual and Other Sensory Neuroprostheses," in *36th Conference on Neural Information Processing Systems (NeurIPS)* (2022).

20. Y. L. Wu, I. Karetic, J. Stegmaier, P. Walter, and D. Merhof, "A Deep Learning-based in silico Framework for Optimization on Retinal Prosthetic Stimulation," in *45th Annual International Conference of the IEEE-Engineering-in-Medicine-and-Biology-Society (EMBC)* (2023).

21. Y. L. Wu, J. Wittmann, P. Walter, and J. Stegmaier, *Optimizing Retinal Prosthetic Stimuli with Conditional Invertible Neural Networks* (2024), arXiv, 1–10.

22. K. Simonyan and A. Zisserman, "Very deep convolutional networks for large-scale image recognition," in *3rd International Conference on Learning Representations* (2015).

23. A. T. Chuang, C. E. Margo, and P. B. Greenberg, "Retinal Implants: A Systematic Review," *British Journal of Ophthalmology* 98 (2014): 852–856, https://doi.org/10.1136/bjophthalmol-2013-303708.

24. M. S. Humayun, J. D. Dorn, L. da Cruz, et al., "Interim Results from the International Trial of Second Sight's Visual Prosthesis," *Ophthalmology* 119 (2012): 779–788, https://doi.org/10.1016/j.ophtha.2011.09.028.

25. M. Farvardin, M. Afarid, A. Attarzadeh, et al., "The Argus-II Retinal Prosthesis Implantation; From the Global to Local Successful Experience," *Frontiers in Neuroscience* 12 (2018): 1–8, https://doi.org/10.3389/fnins.2018.00584.

26. P. Walter, W. Mokwa, and S. Ingebrandt, "Innovative Retinal Interfaces for Optimized Artificial Vision – A New DFG Funded Research Training Group," *Neuroforum* 27 (2021): 99–101, https://doi.org/10.1515/nf-2021-0011.